XLI CILAMCE
XLI Ibero-Latin American Congress on Computational Methods in Engineering
16-19 November, 2020 FOZ DO IGUAÇU PARANÁ – BRAZIL

Error estimations for multiscale hybrid-mixed finite element methods for Darcy's problems on polyhedral meshes

Gustavo A. Batistela[1], Denise de Siqueira[2], Paulo R. Bösing[3], Philippe R. B. Devloo[4], Sônia M. Gomes[5]

[1,4,5]*Universidade Estadual de Campinas*
13083-839, Campinas - SP, Brazil
gustavoabatistela@gmail.com, phil@fec.unicamp.br, soniag@unicamp.br
[2]*Universidade Tecnológica Federal do Paraná*
80230-901, Curitiba - PR, Brazil
denisesiqueira@utfpr.edu.br
[3]*Universidade Federal da Fronteira Sul, Chapecó*
89902-112,SC, Brazil
paulo.bosing@uffs.edu.br

Abstract. A posteriori error estimation for multiscale hybrid-mixed formulations for Darcy's problems is discussed. The method adopts two-scale finite element spaces: refined discretizations are adopted inside polygonal subregions, but flux approximations are constrained over the mesh interfaces by a given coarse normal trace space. For stability, pressure and flux approximations are divergence compatible. The error estimation is based on potential reconstruction, which is a popular technique for this kind of analysis in the context of mixed methods. Numerical experiments are presented in order to illustrate the efficiency of the proposals.

Keywords: Error estimation; multiscale hybrid methods; flux with trace constraints

1 Introduction

Flows in porous media appear in many engineering and environmental applications. The usual characteristics of these applications are their intrinsic multiscale and high-contrast behavior due to heterogeneous coefficients. Under such conditions, the accuracy of standard numerical methods may deteriorate. To improve the performance of simulations, a multiscale treatment is required by some effective technique allowing the incorporation of small scale effects on the larger ones. In this direction, the multiscale hybrid mixed finite element method [1] (denoted by the acronym MHM-H(div) is considered in the current study.

Mixed finite element (FE) methods for Darcy's flows are formulated for flux $\boldsymbol{\sigma}$ and pressure u simultaneously. Flux approximations must have continuous normal traces along inter-element boundaries (i.e. flux FE spaces are H(div)-conforming), but the pressure variable is searched in discontinuous spaces. For stability (inf-sup condition) flux and pressure FE pairs should be divergence-compatible. Local mass conservation occurs and divergence-free constrain can be strongly enforced.

The MHM-H(div) scheme is designed to cope with complex domain geometry and the inherent multiscale nature of the phenomena. It is equivalent to a local-global characterization of a mixed formulation based on a two-scale FE space setting, denoted by MFEM-(γ), where γ represents mesh widths and polynomial degrees of the two-scale levels. The discretizations are based on a general domain partition formed by polyhedral subregions (not necessarily conformal), where a hierarchy of meshes and approximation spaces are considered. The normal traces of the flux over the mesh skeleton (facets of subregion boundaries) are constrained to a given finite-dimensional (coarser) trace space. The FE approximations inside the subdomains may be enriched in different extents: concerning mesh size, polynomial degree, or both. A priori error analysis developed in [1] for this method revealed flux accuracy of order determined by the trace discretizations, despite the resolution increments inside the subregions. However, enhanced accuracy rates for pressure and super-convergent divergence of the flux can be obtained.

The purpose of the current work is to adapt known a posteriori error estimations for standard single-scale mixed methods to the multiscale MHM-H(div) context. We adopt a methodology based on a reconstruction procedure (see [2] for a review on this matter). Given an approximate solution $\boldsymbol{\sigma}$ and u, the principle is to recover a second continuous approximation $s \in H^1(\Omega)$ for pressure (known as *reconstructed potential*) to be used to estimate the unknown exact flux and pressure errors. The algorithm follows two steps: (a) inter-element smoothing,

where a continuous average of the approximate pressure is defined over the mesh skeleton, and (b) the solution of local Dirichlet problems using the interelement average pressure as Dirichlet boundary data.

The outline of the paper is the following. In the next section, the main aspects of the MHM-H(div) scheme for the model problem is summarized. Section 3 is dedicated to the derivation of the desired a posteriori error estimates. In Section 4 a set of numerical examples are presented to verify the efficiency and robustness of our estimates. Finally, we end the paper with some concluding remarks in Section 5.

2 Multiscale Hybrid Mixed Method

Let $\Omega \subset \mathbb{R}^2$ be a polygonal (polyhedral) computational domain with boundary $\partial\Omega = \Gamma_D \cup \Gamma_N \cup \Gamma_R$, with Γ_D, Γ_N and Γ_R being the disjoint parts where Dirichlet, Neumann and Robin boundary conditions are enforced. For simplicity, assume $\Gamma_D \cup \Gamma_R$ has a non-vanishing measure, as a guarantee for solution uniqueness. The model Darcy's problem considers fields for flux $\boldsymbol{\sigma}$ and fluid pressure u defined in Ω satisfying the equations:

$$\begin{aligned} \boldsymbol{\sigma} &= -\mathbb{K}\nabla u, \ \text{ in } \Omega \\ \nabla\cdot\boldsymbol{\sigma} &= f, \ \text{ in } \Omega \\ u = u_D \ \text{ on } \Gamma_D, \ \ \boldsymbol{\sigma}\cdot\mathbf{n}^\Omega &= \sigma_N \ \text{ on } \Gamma_N, \ \ \boldsymbol{\sigma}\cdot\mathbf{n}^\Omega = \alpha_R(u-u_R)+g \ \text{ on } \Gamma_R, \end{aligned}$$

where $\mathbf{n}^\Omega$ is the outward unit normal over $\partial\Omega$, $f \in L^2(\Omega)$, $u_D \in H^{1/2}(\Gamma_D)$, $u_R \in H^{1/2}(\Gamma_R)$, $\sigma_N \in H^{-1/2}(\Gamma_N)$, $g \in L^2(\Gamma_R)$, $\mathbb{K}$ is a bounded symmetric positive definite tensor, and α_R is a continuous, strictly positive function on Γ_R (bounded above and away from zero). Observe that a Neumann condition occurs on $\Gamma_N \cup \Gamma_R$ if $\alpha_R \to 0$, and a Dirichlet condition on $\Gamma_D \cup \Gamma_R$ happens for $\alpha_R \to \infty$. The Robin condition appears for $0 < \alpha_R < \infty$.

2.1 Two-scale mixed FE formulation

Mixed methods for Darcy's flows are formulated as minimization problems constrained by the realization of the divergence equation, and pressure plays the role of the corresponding Lagrange multiplier. Therefore, for stability, the FE pair of spaces for flux and pressure can not be chosen arbitrarily: they should be divergence-consistent. For multiscale applications, the MHM-H(div) scheme is a local-global characterization of a stable mixed formulation using a two-scale FE pair $\mathcal{E}_\gamma = \boldsymbol{V}_\gamma \times U_{\gamma_{in}} \subset \boldsymbol{H}(\mathrm{div},\Omega)\times L^2(\Omega)$, verifying the divergence-constraint $\nabla\cdot\boldsymbol{V}_\gamma = U_{\gamma_{in}}$. The two-scale parameter $\gamma := (\gamma_{sk},\gamma_{in})$, where $\gamma_{sk} = (h_{sk}, k_{sk})$ and $\gamma_{in} = (h_{in}, k_{in})$ are used to indicate the mesh widths and polynomial degrees of the two-scale levels, coarse and refined.

For the FE spaces $\mathcal{E}_\gamma$, consider the mixed FE formulation MFEM(γ): find $\boldsymbol{\sigma} \in \boldsymbol{V}_\gamma$, with $\boldsymbol{\sigma}\cdot\mathbf{n}^\Omega = \sigma_N$ on Γ_N, and $u \in U_{\gamma_{in}}$ such that, for all $\mathbf{q} \in \mathbf{V}_\gamma$, with $\mathbf{q}\cdot\mathbf{n}|_{\Gamma_N} = 0$, and $v \in U_{\gamma_{in}}$, the next equations are verified:

$$\begin{aligned} \int_\Omega \mathbb{K}^{-1}\boldsymbol{\sigma}\cdot\mathbf{q}\,dx + \int_{\Gamma_R}\alpha_R^{-1}(\boldsymbol{\sigma}\cdot\mathbf{n})(\boldsymbol{q}\cdot\mathbf{n}^\Omega)\,ds - \int_\Omega u\nabla\cdot\mathbf{q}\,dx &= \int_{\Gamma_R}(\alpha_R^{-1}g - u_R)(\boldsymbol{q}\cdot\mathbf{n}^\Omega)\,ds \\ &\quad - \int_{\partial\Gamma_D} u_D(\mathbf{q}\cdot\mathbf{n}^\Omega)\,ds, \qquad (1) \\ \int_\Omega \nabla\cdot\boldsymbol{\sigma}\, v\,dx &= \int_\Omega f v\,dx. \qquad (2) \end{aligned}$$

This two-scale formulation is treated in [1] for $\Gamma_D = \partial\Omega$, and the single-scale case for Robin boundary problems $\Gamma_R = \partial\Omega$ is treated in [3, 4]).

Two-scale mesh and FE space setting Let $\mathcal{T} = \{\Omega_i\}$ be a partition of Ω by general non-overlapping polyhedral subdomains Ω_i, and associated to $\mathcal{T}$ define the mesh skeleton Γ formed by the union of the faces $F \in \partial\Omega_i$. Consider a fixed normal vector field $\mathbf{n}$ defined over Γ (i.e., $\mathbf{n}|_{\partial\Omega_i} = \delta\mathbf{n}^{\Omega_i}$, $\delta \in \{1,-1\}$).

Firstly, a coarse single-scale framework is defined satisfying the following properties:

- There is a conformal shape regular partition $\mathcal{T}_{h_{sk}}$ of Ω formed by the union of sub-meshes $\mathcal{T}_{h_{sk}}^{\Omega_i} = \{K\}$ of Ω_i, the elements K having usual triangular or quadrilateral geometry, with characteristic size h_{sk}. A partition $\mathcal{T}_{h_{sk}}^{\Gamma}$ is induced over Γ by $\mathcal{T}_{h_{sk}}$, and for $F \subset \mathcal{T}_{h_{sk}}^{\Gamma} \cap \partial\Omega$ assume $F \subset \Gamma_D$ or $F \subset \Gamma_R$.
- There is a divergent-consistent FE pair $\mathcal{E}_{\gamma_{sk}} = \mathbf{V}_{\gamma_{sk}} \times U_{\gamma_{sk}}$, and a FE space $\Lambda_{\gamma_{sk}}$ defined over Γ by the traces $\mathbf{q}\cdot\mathbf{n}_\Gamma$, $\mathbf{q} \in \mathbf{V}_{\gamma_{sk}}$.

Then, a two-scale setting is formed as follows:

- Refined internal partitions $\mathcal{T}_{h_{in}}^{\Omega_i}$ are obtained by subdivision of $\mathcal{T}_{h_{sk}}^{\Omega_i}$ ($h_{in} \sim h_{sk}/2^\ell$, $\ell \geq 0$), and divergent-consistent FE pairs $\mathcal{E}_{\gamma_{in}}(\Omega_i) = \mathbf{V}_{\gamma_{in}} \times U_{\gamma_{in}}$, based on $\mathcal{T}_{h_{in}}^{\Omega_i}$, are considered for $k_{in} = k_{sk} + n$, $n \geq 0$.
- Two-scale flux FE spaces $\mathcal{E}_\gamma = \boldsymbol{V}_\gamma \times U_{\gamma_{in}}$ are defined: $U_{\gamma_{in}} = \{v \in L^2(\Omega); v|_{\Omega_i} \in U_{\gamma_{in}}\}$, and $\boldsymbol{V}_\gamma = \{\mathbf{q} \in \boldsymbol{H}(\mathrm{div},\Omega); \mathbf{q}|_{\Omega_i} \in \mathbf{V}_\gamma(\Omega_i)\}$, where $\mathbf{V}_\gamma \subset \mathbf{V}_{\gamma_{in}}(\Omega_i)$ refers to constrained vector functions

such that $\mathbf{q}\cdot\ \mathbf{n}|_F \in \Lambda_{\gamma_{sk}}|_F$, for $F \subset \partial\Omega_i \setminus \partial\Omega$. Notice that this flux space with constrained trace is well defined since, by construction, $\Lambda_{\gamma_{sk}} \subset \Lambda_{\gamma_{in}}$, where $\Lambda_{\gamma_{in}}$ is the space of traces induced by $\mathbf{V}_{\gamma_{in}}$ over Γ. The next diagram illustrates some aspects of the two-scale hierarchy of MHM meshes and FE spaces.

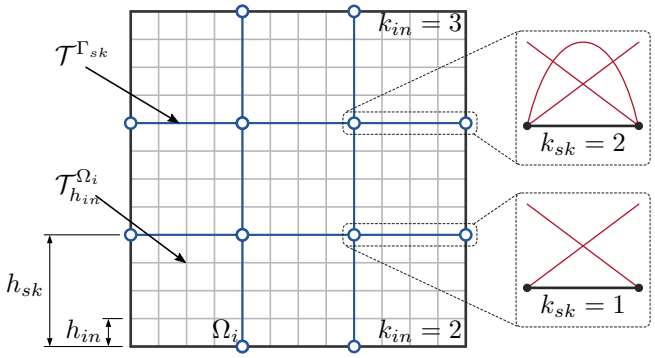

Figure 1. Diagram illustration of a MHM mesh with 3×3 subregions, each being uniformly refined two times, and skeleton edges without subdivision.

For triangular or quadrilateral elements K, FE pairs $\mathbf{V}(K) \times U(K)$ are defined as $\mathbf{V}(K) = \mathbb{F}_K^{\text{div}}(\mathbf{V}(\hat{K}))$ and $U(K) = \mathbb{F}_K(U(\hat{K}))$, backtracking a FE pair $\mathbf{V}(\hat{K}) \times U(\hat{K})$ defined in the master element $\hat{K}$ satisfying $U(\hat{K}) = \nabla \cdot \mathbf{V}(\hat{K})$. The mappings $\mathbb{F}_K$ and $\mathbb{F}_K^{\text{div}}$ are induced by the geometric transformation $F_K : \hat{K} \to K$. Namely, for scalar functions, $p = \mathbb{F}_K\hat{p} = \hat{p} \circ F_K^{-1}$, and for vector functions, $\boldsymbol{v} = \mathbb{F}_K^{\text{div}}\hat{\boldsymbol{v}} = \mathbb{F}_K\left[\frac{1}{\mathbf{J}_K} DF_K\hat{\boldsymbol{v}}\right]$, where DF_K is the Jacobian matrix of F_K, and $\mathbf{J}_K = |\det(DF_K)|$ (Piola transformation). For the current applications, F_K is assumed to be an affine mapping. There exists a variety of stable FE pairs $\mathbf{V}(\hat{K}) \times U(\hat{K})$ used in the construction of flux and potential (pressure) approximations by mixed formulations [5]. Namely, we adopt two families:

- $\mathcal{BDM}_k$ pair for $\hat{K} = \hat{T}$: $V(\hat{K}) = [\mathbb{P}_k(\hat{K})]^2$, $U(\hat{K}) = \mathbb{P}_{k-1}(\hat{K})$,
- $\mathcal{RT}_{[k]}$ pair for $\hat{K} = \hat{Q}$: $V(\hat{K}) = \mathbb{Q}_{k+1,k,k}(\hat{K}) \times \mathbb{Q}_{k,k+1,k}(\hat{K})$, $U(\hat{K}) = \mathbb{Q}_{k,k}(\hat{K})$,

for $k = k_{sk}$ or $k = k_{in}$. The scalar polynomials $\mathbb{P}_k(\hat{K})$ are of total degree at most k, for the triangle $\hat{T}$. For the square $\hat{Q}$, $\mathbb{Q}_{k,t}(\hat{K})$ are the tensor product polynomials of maximum degree k in x and t in y.

Local-global equivalent interpretation This class of two-scale mixed methods was analyzed and implemented in [1] for Dirichlet boundary problems, where an equivalent interpretation in terms of a local-global hybrid approach was established - the MHM-H(div) scheme. It has a divide-and-conquer spirit combined with bubble enrichment techniques and static condensation. In summary, the MHM-H(div) scheme has the following characteristics:

1. There are two operators (upscaling and downscaling) transferring information between the two levels of resolution. They can be interpreted as discrete versions of operators used in a hybrid formulation to characterize the exact solution in terms of components given by well-posed local-global systems.
2. A new trace variable λ (multiplier) is introduced to making the inter-element connection: $\lambda|_F \in \Lambda_{\gamma_{sk}}$ for $F \subset \Gamma \setminus \partial\Omega$, and $\lambda|_F \in \Lambda_{\gamma_{in}}$ for $F \subset \partial\Omega$, λ_{sk} and λ_{in} are coarse and refined FE spaces peacewise defined over the mesh skeleton Γ.
3. An orthogonal decomposition is set for the pressure $u = u_0 + u^{\perp}$ in terms of a coarse component $u_0 \in U_0$, piecewise constant over $\mathcal{T}$, and a fine scale component $u^{\perp}$ in the L^2-orthogonal complement of U_0 in $U_{\gamma_{in}}$.
4. By static-condensation, λ and u_0 are computed by a stable global system (upscaling stage).
5. In the second fine scale, $u^{\perp}$ and $\boldsymbol{\sigma}$ are computed by a set of independent problems restricted to the subregions $\Omega_i \in \mathcal{T}$, taking λ as Neumann boundary data over $\partial\Omega_i$, and using the mixed formulation based on the local FE settings $\mathbf{V}_{\gamma}(\Omega_i) \times U^{\perp}_{\gamma_{in}}(\Omega_i)$, where $U^{\perp}_{\gamma_{in}}(\Omega_i)$ are functions of zero mean in Ω_i. The equations are tested against bubble functions (having support in the corresponding subregion).
6. The downscaling local problems favor the use of parallel strategies.

3 A Posteriori error estimation

A posteriori error estimation is fundamental for efficient error control of numerical simulations. Usually, they give local error indicators defined in terms of the computed approximations and can be used to control the error and/or to adaptively modify the discretization to get the desired accuracy with reduced computational effort [6]. Essentially, some properties are expected for an optimal a posteriori error estimator. Namely, a guaranteed upper bound should be provided, meaning that if η_{Ω_i} denote local error estimations, then $E_{ex} \lesssim E_{est} = \sum_{\Omega_i \in \mathcal{T}} \eta_{\Omega_i}$. The quality of an error estimator is measured by its efficiency index, that is the ratio of the estimated error and

the true error, $I_{eff} = \dfrac{E_{est}}{E_{ex}}$. An error estimator is supposed to be *efficient*, i.e., $I_{eff} \to 1$ as the discretization resolution increases. The local estimators η_{Ω_i} must also be locally efficient, in sense that they provide a lower bound of the local error, $\eta_{\Omega_i} \leq C_{\Omega_i} E_{ex}(\Omega_i)$, for some constant $C_{\Omega_i} > 0$. Finally, η_{Ω_i} have to be computable.

The approach adopted in the current work has been explored in [6–8], for $\Gamma_D = \partial\Omega$, and $u_D = 0$, using a reconstructed potential function $s \in H^1(\Omega)$, obtained from information given by the approximate pressure u.

Theorem 3.1. *Let $(\boldsymbol{\sigma}, u) \in \boldsymbol{V}_\gamma \times U_{\gamma_{in}}$ be the solution of a mixed formulation* (1)-(2)*, and suppose s is a potential reconstruction of u. If $\Pi_{\gamma_{in}} : L^2(\Omega) \to U_{\gamma_{in}}$ is the L^2-orthogonal projection, and $\|\!|\cdot|\!\| = \|\mathbb{K}^{-1/2}(\cdot)\|$ then,*

1. *Upper bound: $\|\!|\boldsymbol{\sigma}_{ex} - \boldsymbol{\sigma}|\!\|^2 \leq \displaystyle\sum_{\Omega_i \in \mathcal{T}} \left(\eta^2_{R,\Omega_i} + \eta^2_{P,\Omega_i}\right)$,*

   where $\eta_{R,\Omega_i} = \dfrac{C_P^{1/2} h_{\Omega i}}{c^{1/2}_{\mathbb{K},\Omega_i}} \|f - \Pi_{\gamma_{in}}(f)\|_{\Omega_i}$, $\eta_{P,\Omega_i} = |\!|\!|\boldsymbol{\sigma} + \mathbb{K}\nabla s|\!|\!|_{\Omega_i}$, C_P is the constant from Poincaré inequality, $c_{\mathbb{K},\Omega_i}$ is the smallest eigenvalue of $\mathbb{K}$ on Ω_i, and h_{Ω_i} is the diameter of the subdomain Ω_i.
2. *Local efficiency: If $\mathcal{T}$ is a regular mesh, it holds for all $\Omega_i \in \mathcal{T}$*

$$\begin{aligned} \eta_{P,\Omega_i} &\leq |\!|\!|\boldsymbol{\sigma}_{ex} - \boldsymbol{\sigma}|\!|\!|_{\Omega_i} + |\!|\!|\mathbb{K}\nabla s - \boldsymbol{\sigma}_{ex}|\!|\!|_{\Omega_i}, \\ \eta_{R,\Omega_i} &\leq \frac{C_P^{1/2} h_{\Omega i}}{c^{1/2}_{\mathbb{K},\Omega_i}} \left[\left(1 + \frac{1}{\tilde{c}_1}\right) \|f - \Pi_{\gamma_{in}}(f)\|_{\Omega_i} + \frac{h^{-1}_{\Omega i}}{\tilde{c}_2} |\!|\!|\boldsymbol{\sigma}_{ex} - \boldsymbol{\sigma}|\!|\!|_{\Omega_i} \right]. \end{aligned}$$

   where $\tilde{c}_i$, $i = 1,\ 2$ are constants that dependent of k_{in} and Ω_i, but are independent of h_{Ω_i}.

The proof of local efficiency follows by using bubble functions and traditional techniques. Notice that error estimates for pressure are stated in [8, Theorem 6.10].

3.1 Potential reconstruction for the two-scale formulation MFEM(γ)

Usually, the auxiliary reconstructed potential s used in the estimators for mixed FE methods can be obtained after three steps [6]: (a) post-processing, solving local Neumann problems by the H^1-conforming formulation based on an enhanced FE space, (b) inter-element smoothing procedure for the pressure, and (c) solution of Dirichlet local problems by the H^1-conforming formulation, taking the smoothed pressure in the boundary data. Notice that for approximations $(\boldsymbol{\sigma}, u) \in \boldsymbol{V}_\gamma \times U_{\gamma_{in}}$ given by the two-scale MFEM(γ) formulation (1)-(2), the pressure is already computed in an enhanced FE space $U_{\gamma_{in}}$. Thus, we better skip the pros-processing step. The steps (b) and (c) adopted in [6] was meant to deal with hp-adaptive mixed FE methods. We adapt them to the more general two-scale settings with FE pairs $\boldsymbol{V}_\gamma \times U_{\gamma_{in}}$. In summary, we define the potential reconstruction as the action of an operator $\mathcal{I} : U_{\gamma_{in}} \to U^c_{\gamma_{in}}$, where $U^c_{\gamma_{in}} \subset H^1(\Omega)$ is locally piecewise defined over $\mathcal{T}^{\Omega_i}_{h_{in}}$, with degree k_{in}.

Inter-element smoothing procedure Let $\mathcal{T}^\Gamma_{h_{in}}$ be the partition induced on Γ by the internal meshes $\mathcal{T}^{\Omega_i}_{h_{in}}$, and define $\Lambda^c_{\gamma_{in}} \subset \Lambda_{\gamma_{in}}$ by the continuous functions piecewisely defined over $\mathcal{T}^\Gamma_{h_{in}}$ by polynomials of degree k_{in}. Given the approximate pressure u given by the MFEM(γ) formulation, the purpose of the inter-element smothing procedure is to construct $\mu \in \Lambda^c_{\gamma_{in}}$, following two consecutive operations.

1. Average over faces $F \subset \mathcal{T}^\Gamma_{h_{in}}$: set $\mu|_F$ according to the following cases:
   - $F = \partial K^i \cap \partial K^j$ with $K^i \in \mathcal{T}^{\Omega_i}_{h_{in}}$ and $K^j \in \mathcal{T}^{\Omega_j}_{h_{in}}$: $\langle (\frac{1}{2}(\omega(K^i)u|_{K^i} + \omega(K^j)u|_{K^j}) - \mu, v\rangle_F = 0, \quad \forall\, v \in \Lambda_{\gamma_{in}}$, where $\omega(K^s), s = i, j$, is the largest eigenvalue of $\mathbb{K}$ on K^s.
   - $F \subset \Gamma_D$: $\langle u_D - \mu, v\rangle_F = 0, \quad \forall\, v \in \Lambda_{\gamma_{in}}$.
   - $F \subset \Gamma_R$: $\langle \underbrace{\alpha_R^{-1}(\boldsymbol{\sigma}\cdot\mathbf{n} - g) + u_R}_{u} - \mu), \varphi\rangle_F = 0, \quad \forall\, v \in \Lambda_{\gamma_{in}}$.
2. Update vertex components: Let $\mathbf{x}_n$ be a vertex of the partition $\mathcal{T}^\Gamma_{h_{in}}$, and set the pach $\mathcal{T}(\mathbf{x}_n) = \{F\}$ of faces $F \in \mathcal{T}^\Gamma_{h_{in}}$ having $\boldsymbol{x}_n$ as one of their vertices. Update the values $\mu(\mathbf{x}_n) \leftarrow \frac{1}{\omega_n} \sum_{F \in \mathcal{T}(\mathbf{x}_n)} \mu|_F(\mathbf{x}_n)$, ω_n being the cardinality of $\mathcal{T}(\mathbf{x}_n)$. Using the hierarchical representation of $\mu|_F$ in terms of vertex and internal shape functions, update the vertex component by interpolating the new vertex values $\mu(\mathbf{x}_n)$, but keep the internal one.

Solving local problems Let $\mu \in \Lambda^c_{\gamma_{in}}$ be given by the inter-element smoothing procedure, and set $\boldsymbol{\sigma}_i := \boldsymbol{\sigma}|_{\Omega_i}$. The potentials $s_i = s|_{\Omega_i}$ are obtained by solving primal FE formulation of local problems in Ω_i using μ to set the boundary data, and FE spaces $U^c_{\gamma_{in}}(\Omega_i) \subset H^1(\Omega_i)$, based on $\mathcal{T}^{\Omega_i}_{h_{in}}$, with degree k_{in}. Namely,

(i) $\partial\Omega_i \cap \partial\Omega = \emptyset$: $s_i \in U^c_{\gamma_{in}}(\Omega_i)$, $s_i|_{\partial\Omega_i} = \mu$, and $(\mathbb{K}\nabla s_i, \nabla w)_{\Omega_i} = -(\boldsymbol{\sigma}_i, \nabla w)_{\Omega_i}, \forall w \in U^c_{\gamma_{in}}(\Omega_i) \cap H^1_0(\Omega_i)$.

(ii) $\partial\Omega_i \cap \partial\Omega \neq \emptyset$: $s_i \in U^c_{\gamma_{in}}(\Omega_i)$, $s_i|_{\partial\Omega_i \setminus (\Gamma_N \cup \Gamma_R)} = \mu$, and $\forall w \in U^c_{\gamma_{in}}(\Omega_i)$, with $w|_{\partial\Omega_i \setminus (\Gamma_N \cup \Gamma_R)} = 0$, the equation $(\mathbb{K}\nabla s_i, \nabla w)_{\Omega_i} + \langle \alpha_R s_i, w\rangle_{\Gamma_R} = -(\boldsymbol{\sigma}_i, \nabla w)_{\Omega_i} + \langle \alpha_R u_R - g + \boldsymbol{\sigma}_i \cdot \mathbf{n}^\Omega, w\rangle_{\Gamma_R}$ holds.

Since $s_i = \mu$ on $\partial\Omega_i \setminus \partial\Omega$, the continuity of s over skeleton interfaces is satisfied, so that $s \in H^1(\Omega)$, as desired.

4 Verification test problems

This section is dedicated to present and discuss some verification tests for a posteriori error estimation based on MHM-Hdiv formulation analyzed in the previous sections.

All the tests are available in the computational framework NeoPZ[1]. The performace of the test are done using:

- The local *effectivity index*, $I_{eff}^{\Omega_i} = \dfrac{\eta_{P,\Omega_i}}{\|\boldsymbol{\sigma}_{ex} - \boldsymbol{\sigma}\|_{\Omega_i}}$;
- The global effectivity index is defined by $I_{eff} = \dfrac{\left(\sum_{\Omega_i} \eta_{P,\Omega_i} + \eta_{R,\Omega_i}\right)^{1/2}}{\|\boldsymbol{\sigma}_{ex} - \boldsymbol{\sigma}\|_{\Omega}}$,

with η_{P,Ω_i} and η_{R,Ω_i} defined in Theorem 3.1.

In all tests, the single-scale FE pair is the Raviart-Thomas $RT_{[1]}$ for quadrilateral elements and Brezzi-Douglas-Marini BDM_1 for triangular elements ($k_{sk} = 1$).

Smooth solution on non-convex subregions Consider a rectangular domain $\Omega = (0,1)^2$ and choose the load function f, such that the exact pressure is given by the smooth function $u(x,y) = \sin(2\pi x)\sin(2\pi y)$. The boundary is configured such that $\partial\Omega = \Gamma_D$, on which a pressure $u_D = u(x,y)|_{\partial\Omega} = 0$ is enforced and the permeability tensor $\mathbb{K}$ is the identity.

The two-scale mesh is created such that, each sub-region is a L-shaped, non-convex geometry (Figure 2 (a)), composed of 3 quadrilateral elements. The edge elements of the skeleton are subdivided accordingly to internal subdivision, so that $h_{in} = h_{sk}$. The polynomial degrees are $k_{sk} = 1$ and $k_{in} = k_{sk} + 3 = 4$.

Figure 2 (b) depicts the behavior of the local effectivity index per sub-region. The global index is $I_{eff} = 1.02561$ as expected indicating that the precision for the error indicator doesn't depend on mesh regularity.

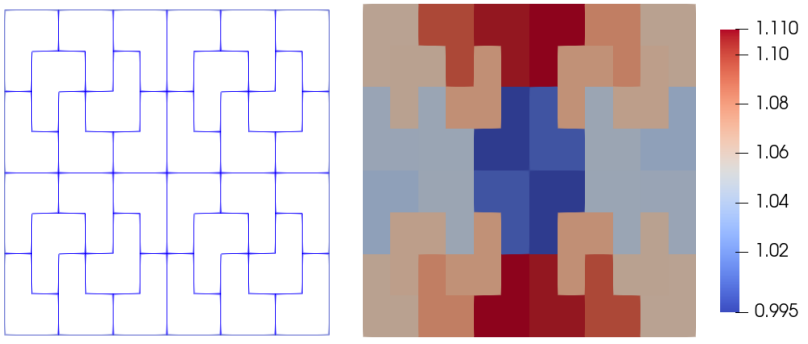

(a) $\mathcal{T}$ (b) $I_{eff}^{\Omega_i}$

Figure 2. Smooth solution: The local effectivity index (b) for non convex mesh (a) expressed in terms of degree of freedom ans using the space configuration $k_{sk} = 1$ and $k_{in} = k_{sk} + 3$.

Singular solution on L- shape domain Our goal here is to study the performance of the error indicator and the effectivity index when the solution has a high gradient. For this purpose we consider the L-shaped domain $\Omega = [-1,1]\times[-1,1] \setminus [0,1]\times[-1,0]$ and the exact solution given by $u(r,\theta) = r^{2/3}\sin(2\theta/3)$ with Dirichlet boundary condition and the permeability tensor $\mathbb{K}$ is the identity. Observe that $u(x,y) \in H^{3/2-\epsilon}$ for all $\epsilon > 0$ and has the singularity at the origin of the L-shaped domain.

There is no mesh subdivision with $h_{in} = h_{sk} = 2^{-3}$, $k_{sk} = 1$ and $k_{in} = k_{sk} + 3 = 4$.

The results for the local exact error and local estimated error per sub-region are plotted in Figure 3. Observed that the biggest values of the exact errors (Figure 3 (a)) and estimated errors (Figure 3 (b)) are around the origin of the domain, where the singularity is located. These results suggest that the error indicator defined on Theorem 3.1 can be used in adaptive process and the adaptive meshes should be refined into this corner.

Figure 4 shows the history of convergence as $h_{sk} \to 0$. As expected, the global effectivity index asymptotically approaches to one.

A synthetic reservoir model For this test we consider the UNISIM-II, a synthetic benchmark reservoir model developed by UNISIM-CEPETRO-Unicamp [9] [2]. The physical configuration is composed of two injection and three production wells that are placed in the domain, with arbitrary pressures of $+20$ and -10 respectively. A homogeneous Neumann boundary condition is imposed in the far-field.

The reservoir is modeled using a triangular mesh, created from the point cloud of UNISIM-II. The geometry was pre-processed from the layers horizons and meshed in an unstructured way (Figure 5 (a)). Every element of

[1] `http://www.labmec.org.br/wiki/neopz/start`

[2] `https://www.unisim.cepetro.unicamp.br/benchmarks/br/unisim-ii/overview`

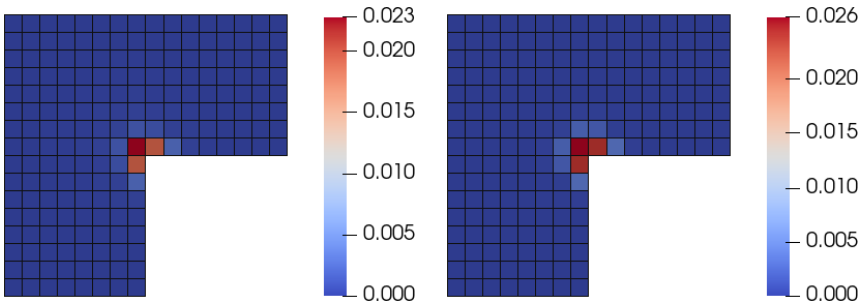

(a) $\|\boldsymbol{\sigma}_{ex} - \boldsymbol{\sigma}\|_{\Omega_i}$ (b) η_{P,Ω_i}

Figure 3. Singular solution: (a) local exact error and (b) estimated error for L-shape mesh using space configurations of type $k_{sk} = 1$ and $k_{in} = k_{sk} + 3$, $h_{in} = h_{sk} = 2^{-3}$.

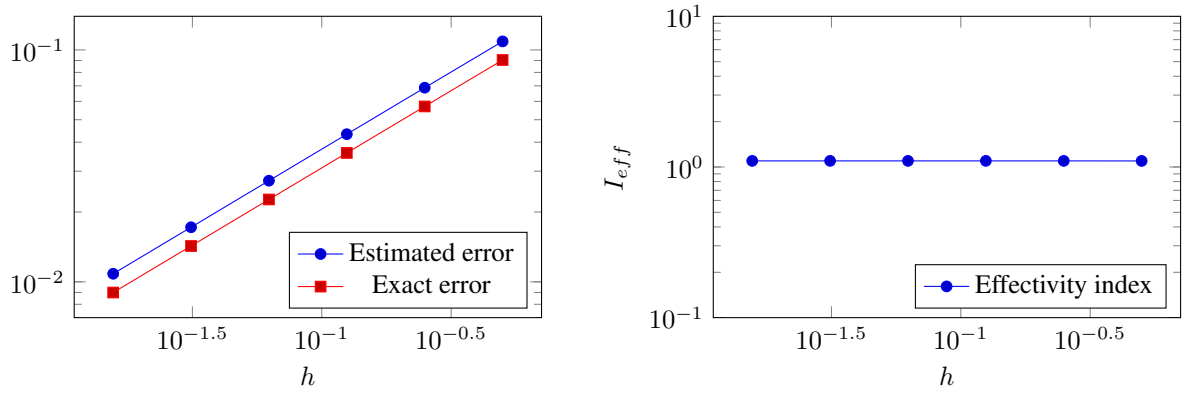

(a) Estimated and exact error (b) Effectivity index

Figure 4. Historic of convergence for the singular problem: In the left side the curve of estimated error (blue line) and exact error (red line), on right side the curve of the effectivity index.

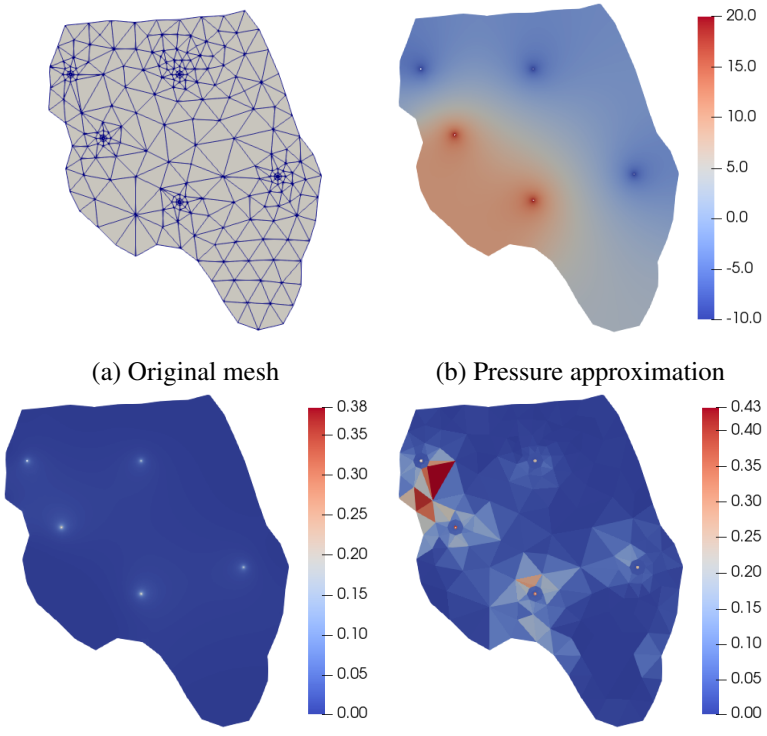

(a) Original mesh (b) Pressure approximation

(c) Flux approximation (d) Local estimator error η_{P,Ω_i}

Figure 5. Results for UNISIM-II problem: Approximation for pressure (b), flux (c) and the local estimated error (c) using the space configuration $k_{sk} = 1$ and $k_{in} = k_{sk} + 1$ and $h_{in} = h_{sk}/4$.

the original mesh define a subregion, which is uniformly refined twice internally, meaning that, $h_{in} = h_{sk}/4$ and the approximation space configuration is $k_{sk} = 1$ and $k_{in} = k_{sk} + 2$ (for the BDM pair this correspond to normal flux degree one, bubble fluxes of degree three and pressure of degree two).

Figure 5 (a) shows the mesh that corresponds to the geometry of the MHM domains: the solution within each MHM triangle is approximated with 16 triangles. Contour plots for pressure and flux are shown in Figure 5 (b) and (c) respectively and the estimated error is plotted in Figure 5 (d).

Even though the results are qualitative, larger errors are estimated in domains that can be intuitively understood. The triangles coloured red (largest errors) are geometrically large elements in a region where the flux varies strongly. The feedback the numerical analyst receives of such estimate can be used to create a more optimized mesh in a straightforward way.

In future research we intend to use the a-priori flow calculations to generate a mesh that is aligned with the flow lines. We expect that the estimated errors for such meshes will be much smaller.

5 Conclusions

The two-scale MHM-H(div) method is formulated for Darcy's problems under general Dirichlet-Neumann-Robin boundary constraints. A posteriori error estimations are applied to control the error of solutions given by this method. Work is in progress to: a) incorporate boundary effects, b) obtain estimations for the trace variable, and c) evalute the estimators for heterogenous media.

Acknowledgements. We gratefully acknowledge the support of EPIC – Energy Production Innovation Center, hosted by the University of Campinas (UNICAMP) and sponsored by Equinor Brazil and FAPESP – São Paulo Research Foundation (2017/15736-3 and EMUs Process and/or scholarship process). We acknowledge the support of ANP (Brazil National Oil, Natural Gas and Biofuels Agency) through the R&D levy regulation. Acknowledgments are extended to the Center for Petroleum Studies (CEPETRO), School of Mechanical Engineering (FEM), and (other Institutes of UNICAMP or other University).

Authorship statement. The authors hereby confirm that they are the sole liable persons responsible for the authorship of this work, and that all material that has been herein included as part of the present paper is either the property (and authorship) of the authors, or has the permission of the owners to be included here.

References

[1] Durán, O., Devloo, P. R. B., M.Gomes, S., & Valentin, F., 2019. A multiscale hybrid method for darcy's problems using mixed finite element local solvers. *Comput Method Appl M*, vol. 354, pp. 213–244.

[2] Vohralík, M., 2015. A posteriori error estimates for efficiency and error control in numerical simulations, *Lecture notes Course NM497*, Universiteé Pierre et Marie Currie - Paris 6.

[3] Roberts, J. E. & Thomas, J.-M., 1991. Mixed and hybrid methods. In Ciarlet, P. G. & Lions, J. L., eds, *Handbook of Numerical Analysis Vol. 2*, pp. 527–639. Elsevier Science Publishers.

[4] Könnö, J., Schötzau, D., & Stenberg, R., 2011. Mixed finite element methods for problems with robin boundary conditions. *SIAM Journal on Numerical Analysis*, vol. 49, n. 1, pp. 285–308.

[5] Boffi, D., Brezzi, F., & Fortin, M., 2013. *Mixed Finite Element Methods and Applications*, volume 44. Springer-Verlag.

[6] Ainsworth, M. & Ma, X., 2012. Non-uniform order mixed fem approximation: Implementation, post-processing, computable error bound and adaptivity. *J Comput Phys*, vol. 231, pp. 436–453.

[7] Ainsworth, M., 2007. A posteriori error estimation for lowest order raviart-thomas mixed finite elements. *SIAM J Sc Comput*, vol. 30, n. 1, pp. 436–453.

[8] Vohralík, M., 2010. Unified primal formulation-based a priori and a posteriori error analysis of mixed finite element methods. *Math Comput*, vol. 79, n. 272, pp. 2001–2032.

[9] Correia, M., Hohendorff, J., Gaspar, A. T. F. S., & Schiozer, D., 2015. UNISIM-II-d: Benchmark case proposal based on a carbonate reservoir. In *SPE Latin American and Caribbean Petroleum Engineering Conference*. Society of Petroleum Engineers.